

# (chiral) Quantum well Rashba splitting in Sb monolayer on Au(111)

Jinbang Hu<sup>1, \*</sup>, Xiansi Wang<sup>2</sup>, Justin W Wells<sup>1,3, \*</sup>

<sup>1</sup>*Department of Physics, NTNU, Trondheim, Norway.*

<sup>2</sup>*Hunan University, Changsha, 410082, China.*

<sup>3</sup>*Semiconductor Physics, Department of Physics, University of Oslo (UiO), NO-0371 Oslo, Norway*

\*Corresponding author: jinbang.hu@ntnu.no; j.w.wells@fys.uio.no.

## Abstract

We present atomic and electronic structure investigations of Single-layer (110) surface of rhombohedral crystal formed Sb on Au(111) substrate. Low energy electron diffraction (LEED) and scanning tunneling microscopy (STM) reveal a pure 2D Sb stripe structure with mirror symmetry broken along the x axis direction. The electronic band structure is determined by angle-resolved photoemission spectroscopy (ARPES). The significantly complex surface band structure results from a combination of a surface band originating from the three different azimuthal orientations of the (110) rhombohedral phase and Umklapp scattered branches of Au sp band. The experimental bands are compared to the calculated band structure of  $3 \times \sqrt{3}$  periodicity of Sb(110). Most of the experimental band dispersions are qualitatively reproduced by the theoretical band structure except Umklapp scattered surface band. Taking advantage of our DFT calculations, we found the quantum well (QW) Rashba splitting bands appear at both  $\bar{\Gamma}$  point and  $\bar{X}$  point. Considering the surface Brillouin zone (SBZ) relationship between Sb(110) sub-unit cell and Au(111) surface, the distinct in energy position of QW states at  $\bar{\Gamma}$  point and  $\bar{X}$  point is found be a combination of the relative spin-orbital coupling (SOC) and the buckling of Sb monolayer on Au surface that work together. The orbital decomposition of the Sb(110) projected band structure indicates hybridization between Sb py state and Au state can modify the spin splitting of QW states due to the intrinsic large SOC of Au state introduced into the QW states.

## INTRODUCTION

Manipulation of the spin degrees of the 2D gas confined in the ultrathin metal film plays an important role in the rapidly developing field of spintronics<sup>1-2</sup>. As the Rashba effect predicted by the theory, lifting of spin degeneracy originates from the spin-orbit coupling (SOC) in inversion symmetry broken structures<sup>3</sup>. The structural inversion asymmetry can be induced by a perpendicular and an in-plane component of the surface-potential gradient from the substrate, leading to the spin splitting of the surface band structure, which is further enhanced by the atomic SOC from the material.

In recent years, a class of 2D surface alloys has been successfully fabricated on noble metal surface by substitution one out of three atoms within the topmost (111) surfaces forming a  $\sqrt{3} \times \sqrt{3}$  periodicity, for example, Pb, Bi, and Sb grown on Ag(111) and Cu(111), Sn on Au(111)<sup>4-10</sup>. Interestingly, free-electron-like surface states with the largest known Rashba spin splitting was reported for Ag<sub>2</sub>Bi, and a number of prior studies of the 2D surface alloy have confirmed the important role played by the atomic SOC in determining the strength of the splitting and also the atomic corrugation of the top atomic layer. However, the electronic property of 2D adlayer, so far, have rarely been well discussed with symmetry being considered. Note that there is a giant spin-orbit splitting of quantum-well states in the surface state of a Bi monolayer on Cu(111) reported from previous angle resolved two-photon-photoemission measurements and calculations<sup>11</sup>. Similarly, like the Rashba splitting observed in 2D surface alloys, the ultrathin metal films as a tunable quantum-well (QW) systems also exhibits spin-orbit splitting of the electronic states induced by the asymmetric confinement due to the surface potential and the interface potential.

Apart from the easily preparation of a long-range ordered surface alloy superstructure, the single layer material may form several different reconstructions, also the rotational of the domain determined by the symmetry of the substrate, end in extremely complicated 2D surface band structure collected by ARPES. In the present work, we introduce a method for disentangling the complicated surface electronic structure. We have studied the origin of the intrinsic 2D surface band from Sb(110) rhombohedral phase and also the important role of symmetry broken played with the atomic orbital

hybridization in determining the Rashba splitting strength of the Quantum well states. Our further analysis indicates both the 2D Sb stripe structure from STM observation and QW states confirmed by ARPES shows the chiral character.

### EXPERIMENTAL AND THEORETICAL DETAILS

All sample preparation steps and experiments were performed under ultrahigh vacuum conditions. The Au(111) surface was prepared by repeated sputtering and annealing cycles. The quality of the clean surface was confirmed by the STM observation of the well-known Au-herringbone reconstruction. (Fig. S1) Subsequently, Sb (purity 99.9999%) was deposited onto the clean surface at room temperature, yielding a single (110) rhombohedral phase. During the evaporation, the pressure remained better than  $4 \times 10^{-10}$  mbar. The success of the sample preparation was confirmed by Low Energy Electron Diffraction (LEED). All photoemission, and LEED experiments were performed in the chambers at room temperature with base pressures better than  $4 \times 10^{-10}$  mbar. Band structure measurements were performed at  $T \approx 115$  K using an aberration-corrected, energy-filtered photoemission electron microscope (EF-PEEM) (NanoESCA III, Scienta Omicron GmbH) equipped with a focused helium discharge lamp primarily generating He I photons at  $h\nu = 21.22$  eV, using pass energy  $EP = 25$  eV and a 0.5 mm entrance slit to the energy filter, yielding nominal energy and momentum resolutions of  $\Delta E = 50$  meV and  $\Delta k = 0.02$   $^\circ \text{\AA}^{-1}$ .

The density functional theory calculations were performed using the Vienna Ab initio Simulation Package (VASP)<sup>13</sup>. The interactions between the valence electrons and ion cores were described by the projector augmented wave method<sup>14</sup>. The electron exchange and correlation energy were treated by the generalized gradient approximation with the Perdew-Burke-Ernzerhof functional<sup>15-16</sup>. The kinetic energy cutoff of the plane-wave basis was set to 500eV as default. For the matched models, The first Brillouin zone of single-layer Sb(110) on Au(111) system was sampled with the  $\Gamma$ -centered  $6 \times 6 \times 1$  k points. The structures were optimized with symmetry (space group PM) until the forces on the atoms were less than  $10 \text{ meV} \text{\AA}^{-1}$ . The Au(111) surface was described by a periodic slab separated by 15  $\text{\AA}$  vacuum. 15 layers of Au atoms were included with the bottom 12 layers fixed as the bulk crystal structure while the top three layers were relaxed. One monolayer of Sb atoms was adsorbed on top side of the Au slab. In order to "unfold" the band structure with the symmetry of the primitive unit cell of SL Sb(110) and also the Au(111), we have calculated the effective band structure proposed by Popescu and Zunger<sup>17</sup> as implemented in the BandUp code<sup>18-19</sup>. Spin-orbit coupling has been included for all band structure calculations.

### RESULTS AND DISCUSSION

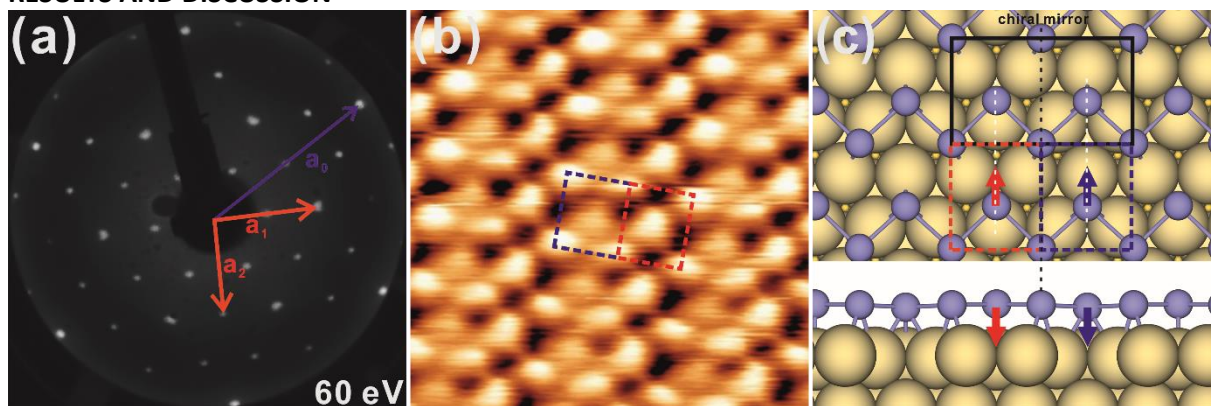


Fig. 1. (a) LEED pattern of 2D Sb film grown on the Au(111) substrate taken at the beam energy of 60 eV. The reciprocal unit cell vectors of Au(111) and Sb reconstruction are indicated with blue arrow  $a_0$ , and red arrow  $a_1$ ,  $a_2$  respectively. (b) STM investigation of the Sb stripe with a  $3 \times \sqrt{3}$  superstructure on Au(111). The two adjacent Sb(110) unit cell marked by the blue and red dashed rectangular. (c) top and side view of fully optimized slab lattice of the Sb stripe superstructure, the blue and red arrow overlaid on two Sb atoms in two adjacent unit cell to explain the potential they experienced, three dashed line indicate the mirror axes for the mirror symmetry of the Sb(100) unit cell and potential of the two Sb atom at the quasi-hcp on Au(111). Scanning parameters: (b) -1.5V, 0.9 nA;

Fig.1 summarizes the monolayer (110) surface of rhombohedral crystal fabricated by epitaxial growth of Sb on a Au(111) surface. As the deposition process approaches completion for a monolayer (ML)

configuration, new spots appear in the LEED pattern shown in both Fig.1(a), where 12 spots inside the  $Au(1 \times 1)$  spots are located on three rotated rectangular unit cell of Sb(110) ML on Au(111) surface. In fact, it has been reported for the case of Sb stripe with a  $3 \times \sqrt{3}$  superstructure formed on the Au(111) surface that four Sb atoms within the rectangular unit cell, differing in their respective heights.<sup>12</sup> However, our analysis is that the current atomic model is not apt, as evidenced by the incongruity in the simulated STM image's brightness between Sb1 and Sb3 atoms, which contrasts with the observed STM findings that indicate a similar brightness.

In our study, we report rectangular supercell of the Sb stripe with the mirror symmetry. The theoretically optimized structure of Sb on Au(111) is depicted in Fig. 1(c). Notably, the region displaying a brighter stripe ribbon corresponds to three higher-positioned Sb atoms, clearly visible in the side view of the optimized lattice. On closer inspection, the Sb stripe superstructure can be divided into two Sb(110) sub-unit cells, represented by the red and blue dashed rectangles, respectively. One of these sub-unit cells exhibits an upward buckle towards the vacuum, with the central Sb atom within the rectangle slightly elevated above the adjacent Au atom. In contrast, the other sub-unit cell exhibits a buckle towards the Au(111) substrate side. This distinctive positioning of the two Sb atoms within the Sb(110) sub-unit cell accounts for the prominent bright stripe ribbon evident in the STM image(Fig. 1(b))<sup>[12]</sup>.

From the geometrical structure of Sb monolayer on Au(111), this commensurate rectangular  $3 \times \sqrt{3}$  stripe superstructure can also be expressed in its matrix form as  $\begin{pmatrix} 3 & 0 \\ 1 & 2 \end{pmatrix}$  referring to Au(111) surface or  $\begin{pmatrix} 2 & 0 \\ 0 & 1 \end{pmatrix}$  referring to Sb(110) rectangle unit cell. In Fig 1(c), It can also be expected that the Sb atom, marked by the arrow, in the centre of two adjacent Sb(110) unit cell experience a potential gradient along the y direction due to each Sb(110) unit cell representing a mirror symmetry along the y direction. The mirrored plane is marked by the white dashed line in Fig 1(c). In the perspective of the  $3 \times \sqrt{3}$  stripe superstructure, an additional mirror symmetry aligned with the y-axis can be invoked to illustrate the presence of chiral symmetry, represented by the black bashed line Fig 1(c), with regard to two adjacent Sb(110) unit cell. The manifestation of chiral symmetry is also evident in the electronic properties, which will be expounded upon in the subsequent discussion.

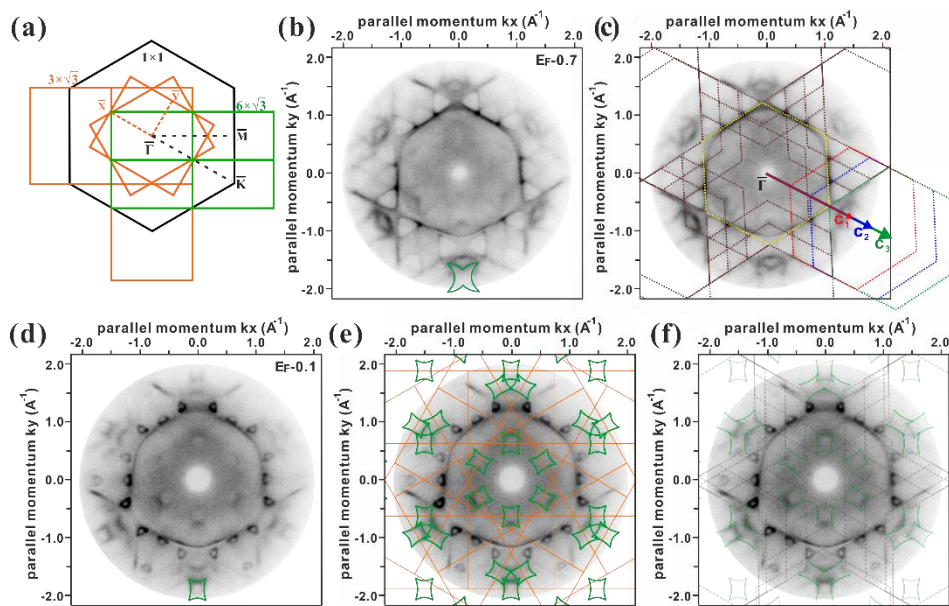


Fig. 2. (a)  $1 \times 1$ , Sb(110) and  $3 \times \sqrt{3}$  surface Brillouin zone scheme for Au(111) surface, Sb(110) rhombohedral unit cell and Sb stripe superstructure. (b) constant energy contours from the Sb/Au(111)  $3 \times \sqrt{3}$  surface at 115K. The contours are shown at 0.7eV(b) and 0.1eV(d) below the fermi level. The new appearing surface band marked as green flower. (c) dashed hexagon (in brown) drawn to trace the weak features appearing in the constant energy contours. The weak dashed hexagon originates from Umklapp scattering of Au sp band, marked by the bright dashed hexagon (in yellow). Three reciprocal lattice vectors marked as C1, C2 and C3 indicate the possible Umklapp scattering

process. (e) Sb(110) SBZ with green-line marks appearing at  $\bar{X}$  point overlaid on the constant energy contours to trace the possible position of flower-shaped bands. (f) Umklapp scattering of Au sp band, combined with flower marks from the three different azimuthal orientations of the (110) rhombohedral phase fits on the constant energy contours.

We now turn to the electronic structure investigated by ARPES, using a focused helium discharge lamp primarily generating He I photons at  $h\nu = 21.22$  eV. Fig. 2 shows the constant energy contours obtained from the Sb/Au(111)  $3 \times \sqrt{3}$  surface. In this section, we use constant energy contours at 0.7 eV below the Fermi level as an example to delve into a detailed electronic structure study of Umklapp scattering originating from Au sp band. Additionally, we employ a constant energy contour at 0.1 eV to elucidate the complex Umklapp scattering band induced by the three different azimuthal orientations of the Sb(110) rhombohedral phase on the Au(111) surface. Fig. 2(a) presents the  $1 \times 1$  (black hexagon), Sb(110) (yellow rectangle) and  $3 \times \sqrt{3}$  (green rectangle) SBZ schemes for Au(111) surface, Sb(110) rhombohedral unit cell and Sb stripe superstructure. The three overlaid yellow rectangles indicate three rotational domains of Sb(110) rhombohedral unit cell, extending across the 1st Au(111) SBZ. According to the radius of Sb(110) SBZ discussed above, the radius along  $\bar{\Gamma} - \bar{Y}$  direction of Sb  $3 \times \sqrt{3}$  SBZ is half length as  $a_2/2$  due to the Sb stripe supercell is twice as the size of Sb(110) unit cell along the direction perpendicular to the stripe. As we can see from Fig. 2(b) and 2(d), the triangle-shaped feature appears at the  $\bar{K} - \bar{M}$  direction of Au(111) SBZ and its size gradually decreases as the binding energy approaches the Fermi level. In Fig. 2(c), the Au(111) sp band is marked with yellow dashed hexagons. To understand the origin of the weak triangle features around the  $\bar{K}$  point of Au(111) SBZ, we have drawn brown dashed hexagons to trace the band features observed in the experimental constant energy contours. These brown dashed hexagons can be categorized into three groups, originating from three different Umklapp scattering processes with reciprocal lattice vectors marked as  $C_1$  (in red),  $C_2$  (in blue) and  $C_3$  (in green), respectively. A careful analysis reveals that  $C_1 = 4a_1 - a_2$ ,  $C_2 = 3a_2$ ,  $C_3 = 4a_1$ . Notice, we only use three types of Umklapp scattering vectors to set an example as fitting well with the weak triangle bands in experimental constant energy contours, there is highly possible of extra Umklapp scattering vectors being applied to tracing the triangle band feature in higher order SBZ of Au(111) surface, as well as the fuzzy background in the first Au(111) SBZ. More further, the influence from three rotational domains of Sb(110) rhombohedral lattice has also been discussed to disentangling the flower-shaped band (marked by green line in Fig. 2(b,d)), which can't be ascribed solely to the Umklapp scattering of Au sp band. Fig. 2(e) represents the constant energy contour at the binding energy 0.1 eV overlaid by the orange rectangle of Sb(110) SBZ with the flower-shaped band located at  $\bar{X}$  point. The new schematic drawing of flower-shaped bands agrees well with the experimental band features appearing at two sides of  $\bar{M}$  points along  $\bar{\Gamma} - \bar{M}$  direction of Au(111) SBZ. Ultimately, Fig. 2(f) confirms the veracity of the novel schematic rendering of the flower-shaped bands, harmoniously aligned with the encompassing larger hexagon-traced Umklapp pattern, thus eloquently corroborating the nature of the complicated surface bands feature engendered by the Sb/Au(111)  $3 \times \sqrt{3}$  surface. The well agreement of the Umklapp scattering band fitting with the complicated feature in ARPES data indicates the well-ordered Sb(100) rhombohedral unit cell formed in a 2D Sb film on Au(111).

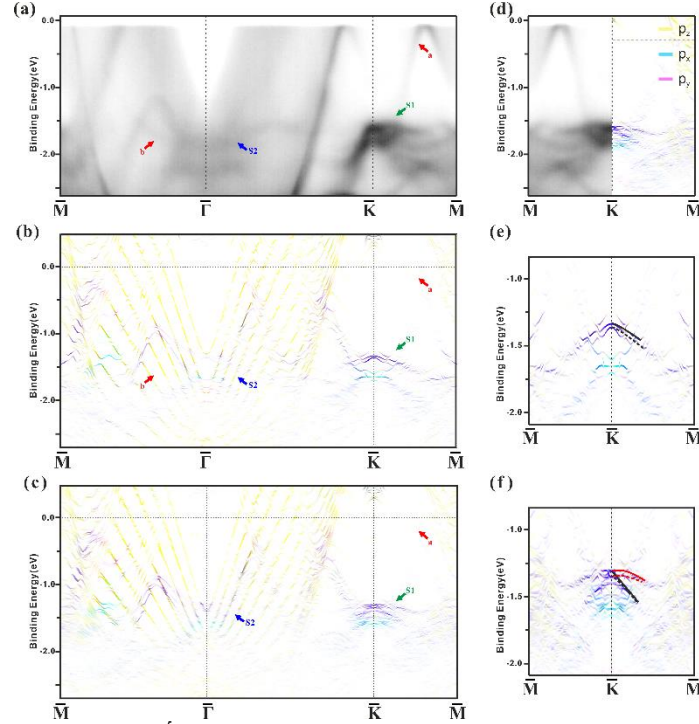


Fig. 3. ARPES results from the Sb/Au(111)  $3 \times \sqrt{3}$  surface along high-symmetry directions of the Au(111) SBZ. Dispersive features labelled b originate from three-dimensional bulk bands of Au(111). The labels S1 and S2 are used to denote the bands originating from the 2D Sb(110) reconstruction. The label a originates from Umklapp scattering of Au sp band. Calculated band structure without SOC (b) and with SOC (c) for the  $3 \times \sqrt{3}$  model of the Sb/Au(111) surface reconstruction shown in Fig. 1(c). yellow, blue, pink and purple symbols show contributions from  $p_z$ ,  $p_x$ ,  $p_y$  and  $p_x+p_y$  states, respectively. (d) comparison between ARPES data and calculated band dispersion along  $\bar{K} - \bar{M}$  direction. The calculated bands shifted up by 0.2 eV to match the ARPES data. (e-f) comparison between calculated band dispersion along  $\bar{K} - \bar{M}$  direction without SOC (e) and with SOC (f) around  $\bar{K}$  point to illustrate the splitting of two pair of Rashba-type bands.

To gain further insight into the electronic structure of the Sb/Au(111)  $3 \times \sqrt{3}$  surface and to elucidate the origin of the large Rashba-type spin-orbit splitting observed within this system, band structure calculations were performed based on DFT as previously expounded. The  $3 \times \sqrt{3}$  model for the periodized stripe structure is applied based on the LEED pattern and STM observations<sup>12</sup>. Fig. 3(b) and 3(c) show such weighted band structure without SOC (b) and with SOC (c) projected from Sb(110) single layer. The symbols colored in yellow, blue, and pink represent contributions from  $p_z$ ,  $p_x$ , and  $p_y$  states, respectively. The calculated bands with SOC, as displayed in Fig. 3(c), exhibit a good overall agreement with the experimental bands in Fig. 3(a), apart from the bands labeled as 'a' and 'b'. The feature a presents a discernibly akin band dispersion to that of the Au sp band, and its conspicuous absence within the calculated band structure correlates with our ascertained deduction of its origin emanating from Umklapp scattering of the Au sp band. There are two new band features, S1 and S2, appearing. The band S1 appears with a strong photon emission intensity around the  $\bar{K}$  point as a maximum energy at 1.55 eV below the fermi level. And several branches of S1 band disperses downward away from the  $\bar{K}$  point, while the band feature S2 shows a blurry dispersion in  $\bar{\Gamma} - \bar{K}$  direction of Au(111) SBZ, due to the overlapping with the replicas of the Au bulk band feature b, resulting from photoexcitation by the He I  $\beta$  emission line of the nonmonochromatized He I light source. We now turn to our discussion with the surface band structure projected onto the Sb(110) topmost layer, unfolding along the  $\bar{K} - \bar{M}$  direction of Au(111) SBZ. We can clearly identify experimentally observed surface band S1 with several branches in our calculations with considering SOC (Fig. 3(c), also a directly comparison in Fig. 3d). Comparing to the calculated bands without considering SOC in Fig. 3(e), we elucidate a distinct morphological transformation of band feature S1 as the division into two discernible parabolic sub-bands along  $\bar{K} - \bar{M}$  direction when SOC is included in the DFT calculations (Fig. 3(f)). There is a small splitting in energy of the S1 band around the  $\bar{K}$  points without SOC in Fig. 3(c), and the separation of the two subband is further enhanced after SOC being considered.



which is due to the two sub-unit cells Sb(110) in the stripe superstructure buckling oppositely normal to Au(111) surface. Our further calculation of the Sb/Au(111)  $3 \times \sqrt{3}$  surface without buckling of the stripe superstructure confirmed the obviously decreasing separation of the two branch of S1 band(Fig. S2). We then deduce the small energy discrepancy of the two pair of Rashba-type bands is a combined contribution from SOC and bulking of Sb stripe structure.

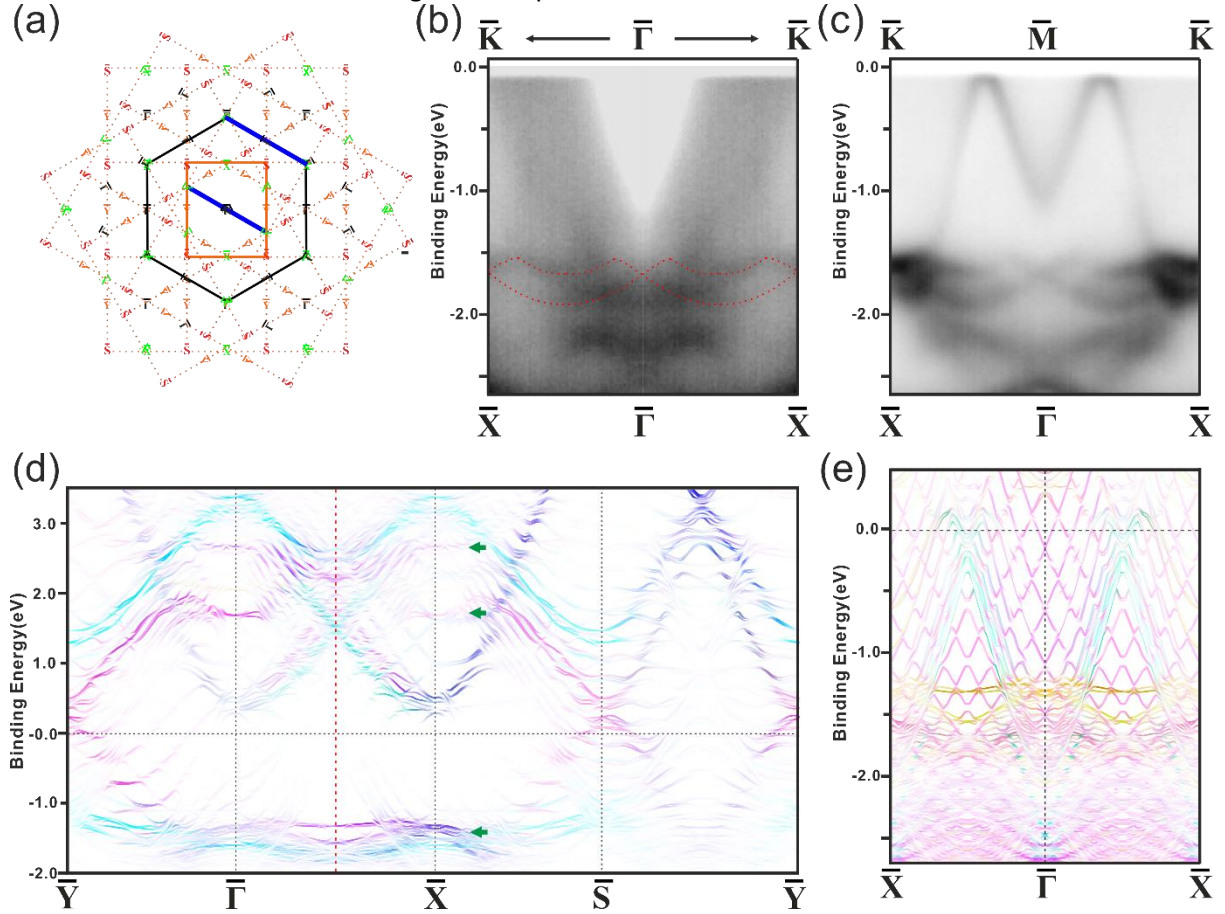


Fig. 4. (a) the distribution of SBZ of the Sb(110) rectangular sub-unit cell extending over the SBZ of Au(111), the high symmetry point symbolled by  $\bar{\Gamma}$ ,  $\bar{X}$ ,  $\bar{Y}$ , and  $\bar{S}$  to mark the location of corresponding band structure around the high symmetry point. (b-c) ARPES results from Sb/Au(111)  $3 \times \sqrt{3}$  surface along high-symmetry directions marked as blue line in (a), the red dashed pattern used to trace the weak S2 band discussed in Fig. 3(a). (d). calculated band structure unfolded to SBZ of Sb(110) sub-unit cell, light blue and pink symbols show contributions from px, and py states of Sb topmost layer, respectively. The green arrow used to mark the energy position of QW states. (e) calculated band structure projected from the topmost Au layer to show the contribution from Au dz2 (weighted by yellow) in the occupied QW state.

Fig. 4(a) shows the SBZ of the Sb(110) unit cell extending over the SBZ of Au(111), the high symmetry point symbolled by  $\bar{\Gamma}$ ,  $\bar{X}$ ,  $\bar{Y}$ , and  $\bar{S}$  to mark the band structure around the corresponding high symmetry point. Due to the three different azimuthal orientations of the Sb(110) rhombohedral phase and the distinct in lattice parameters between Au(111) surface and Sb(110) sub-unit cell, we found the band feature  $\bar{\Gamma}$  and  $\bar{X}$  meet at the  $\bar{K}$  symmetry point of Au(111) SBZ, and the same feature  $\bar{\Gamma}$  (symbol used as a mark of the band structure around  $\bar{\Gamma}$  point) from the 2nd SBZ of Sb(110) sub-unit cell appears independently at the  $\bar{M}$  symmetry point of Au(111) SBZ.

Based on the distribution of SBZ of Sb(110) on Au(111) substrate, Fig. 4(b) and 4(c) show the band dispersion along the high symmetry path labelled by the blue line in Fig. 4(a), we can see the surface band, marked by the red dashed line in Fig. 4(b), shielded by the Au bulk state repeats clearly around the  $\bar{M}$  symmetry point of Au(111) SBZ, which shares the same position with  $\bar{\Gamma}$  symmetry point of the 2nd Sb(110) SBZ as we discussed. Remarkably, in Fig. 4(c), it seems the feature of the Rashba-type splitting band connecting between  $\bar{\Gamma}$  and  $\bar{X}$  points show a mirror symmetry with a mirrored plane positioned at the midpoint and perpendicular to the  $\bar{\Gamma} - \bar{X}$  Brillouin path. This mirror symmetry

relates to the mirror symmetry of the potential experienced in the two adjacent Sb(110) rectangular sub-unit cell, which will be discussed below. This mirror-symmetry Rashba-type splitting band shows a stronger intensity of the band crossing around the  $\bar{X}$  points than the crossing at  $\bar{\Gamma}$  points, due to the signal from the  $\bar{\Gamma}$  symmetry point meeting with the signal from the another two  $\bar{X}$  symmetry point in the 2<sup>nd</sup> Sb(110) SBZ (shown in Fig. 4(a)). Carefully checking the energy of the crossing point at  $\bar{X}$  point and  $\bar{\Gamma}$  point in Fig. 4(c), it can be found that the binding energy of the Rashba splitting band at  $\bar{\Gamma}$  point is slightly higher than at  $\bar{X}$  points, which is in agreement with the energy separation of the two pair of Rashba-type band appearing at  $\bar{K}$  point of Au(111) SBZ, shown in Fig. 3 (e-f).

As we claimed three mirrored planes in the stripe superstructure perpendicular to x axis and the nice agreement between the DFT calculated band structure and ARPES data, we do a further analysis the role of in-plane potential gradient along the y direction played on band structure. The absence of mirror symmetry perpendicular to the y-axis engenders a potential gradient along the y-direction. This gradient, in turn, serves as the driving force behind the possible emergence of Quantum Well (QW) states originating from the Sb py orbitals. Fig. 4(d) shows the band structure unfolded to SBZ of Sb(110) sub-unit cell. Light blue and pink symbols show contributions from px and py states of Sb topmost layer, respectively. The QW states, marked by the green arrow in Fig. 4(d), at three different energy level can be clearly observed at  $\bar{X}$  symmetry point and another three QW states at  $\bar{\Gamma}$  point, respectively. The projected px and py states along the  $\bar{Y} - \bar{\Gamma} - \bar{X} - \bar{Y}$  direction, overall, show a mirror symmetry, the mirror marked by the red dashed line, which indicates the chiral properties of the three pair of QW states at  $\bar{X}$  point and  $\bar{\Gamma}$  point.

On contrary to the reported increasing spin splitting of QW states with the level of their binding energy in Bi(110) monolayer on Cu(111) system<sup>11</sup>, the QW states of Sb monolayer on Au(111) surface shows a inversely tendency of the Rashba spin splitting. Since Sb shows intrinsically weak SOC while SOC in Au is strong, the degree of the Rashba spin splitting in different level of QW states can be modified by hybridization with Au states. Besides the character of Sb py orbital appearing in the QW states, orbital decomposition of calculated band structure projected from the topmost Au layer indicates the contribution from the Au orbital. As we can see in Fig. 4(e), the occupied QW state at -1.35eV shows a strong py-dz<sup>2</sup> orbital hybrid character, the unoccupied QW state at 1.7eV shows a py-px orbital character while the QW state at 2.7eV shows a weak hybrid character with Au states. Even though the higher QW state shows the tendency of increasing delocalization towards the vacuum due to the effective lowering of the vacuum barrier for the higher-lying states, we deduce the SOC plays a more important role in Rashba spin splitting degree.

## SUMMARY

In our Letter we show a method to disentangle the intrinsic Sb(110) band from Umklapp scattered branches of Au sp band and the three different azimuthal orientations of the (110) rhombohedral phase. Further, we show the giant Rashba splitting appearing at  $\bar{\Gamma}$  and  $\bar{X}$  symmetry point, our findings are fully confirmed by first-principles electronic structure calculations. The discrepancy in binding energy between Rashba splitting band at  $\bar{\Gamma}$  point and  $\bar{X}$  point is caused by a combined contribution from SOC of Au and bulking of Sb stripe structure. The mirror symmetry of Sb stripe structure confirmed by STM observation and calculation predicts the sign of chiral QW states due to the in-plane potential gradient along the y direction appearing in two adjacent Sb(110) unit cell. We also explained the important role of strong spin-orbital coupling within the Au states played in hybridization with Sb py state to modify the spin splitting of QW states.

## ACKNOWLEDGMENT

This work was partially supported by the Research Council of Norway through its Centres of Excellence funding scheme, Project No. 262633, "QuSpin". X. S. W. acknowledges support from the Natural Science Foundation of China (NSFC) Grant No. 12174093 and the Fundamental Research Funds for the Central Universities.

## REFERENCE:

- 1 Anjan, S. et al. Emergent phenomena induced by spin–orbit coupling at surfaces and interfaces. *Nature* **539**, 509 (2016).
- 2 Manchon, A. et al. New perspectives for Rashba spin–orbit coupling. *Nat. Mater.* **14**, 871 (2015).
- 3 Rashba, E. et al. Properties of semiconductors with an extremum loop. 1. Cyclotron and combinational resonance in a magnetic field perpendicular to the plane of the loop. *Sov. Phys. Solid State* **2**, 1109 (1960).
- 4 Pacilé, D. et al. Electronic structure of an ordered Pb/Ag(111) surface alloy: Theory and experiment. *Physical Review B* **73**, 245429 (2006).
- 5 Moreschini, L. et al. Assessing the atomic contribution to the Rashba spin-orbit splitting in surface alloys: Sb/Ag(111). *Physical Review B* **79**, 075424 (2009).
- 6 Christian, R. et al. Giant Spin Splitting through Surface Alloying. *Physical Review Letters* **98**, 186807 (2007).
- 7 Maniraj, M. et al. Structure and electronic properties of the (3×3) R30° SnAu<sub>2</sub>/Au (111) surface alloy. *Physical Review B* **98**, 205419 (2018).
- 8 Shah, I. et al. Atomic and electronic structures of the Au<sub>2</sub>Sn surface alloy on Au(111). *Physical Review B* **104**, 125408 (2021).
- 9 Mirhosseini, H. et al. Unconventional spin topology in surface alloys with Rashba-type spin splitting. *Physical Review B* **79**, 245428 (2009).
- 10 Hendrik, B. et al. Spin orientation and sign of the Rashba splitting in Bi/Cu(111). *Physical Review B* **84**, 115426 (2011).
- 11 Mathias, S. et al. Quantum-Well-Induced Giant Spin-Orbit Splitting. *Physical Review Letters* **104**, 066802 (2010).
- 12 Cantero, E. D. et al. Synthesis and characterization of a pure 2d antimony film on au (111). *The Journal of Physical Chemistry C* **125**, 9273 (2021).
- 13 Kresse, G. & Joubert, D. From ultrasoft pseudopotentials to the projector augmented-wave method. *Physical Review B* **59**, 1758 (1999).
- 14 Blöchl, P. E. Projector augmented-wave method. *Physical Review B* **50**, 17953 (1994).
- 15 Perdew, J. P., Burke, K. & Ernzerhof, M. Generalized gradient approximation made simple. *Physical Review Letters* **77**, 3865 (1996).
- 16 Perdew, J. P., Burke, K. & Ernzerhof, M. Generalized Gradient Approximation Made Simple [Phys. Rev. Lett. 77, 3865 (1996)]. *Physical Review Letters* **78**, 1396 (1997).
- 17 Popescu, V. et al. Extracting E versus k effective band structure from supercell calculations on alloys and impurities. *Physical Review B* **85**, 085201 (2012).
- 18 Paulo, V. C. et al. Effects of extrinsic and intrinsic perturbations on the electronic structure of graphene: Retaining an effective primitive cell band structure by band unfolding. *Physical Review B* **89**, 041407 (2014).
- 19 Paulo, V. C. et al. Unfolding spinor wave functions and expectation values of general operators: Introducing the unfolding-density operator. *Physical Review B* **91**, 041116 (2015).

## Supporting information

### (chiral) Quantum well Rashba splitting in Sb monolayer on Au(111)

Jinbang Hu<sup>1, +</sup>, Xiansi Wang<sup>2</sup>, Justin W Wells<sup>1,3, +</sup>



<sup>1</sup>Department of Physics, NTNU, Trondheim, Norway.

<sup>2</sup>Hunan University, Changsha, 410082, China.

<sup>3</sup>Semiconductor Physics, Department of Physics, University of Oslo (UiO), NO-0371 Oslo, Norway

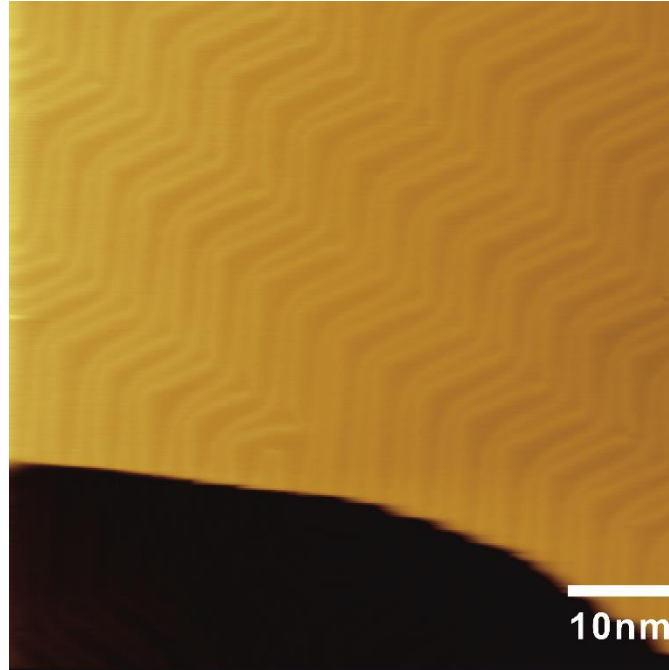


Fig. S1 STM image of clean Au(111) surface before Sb deposition. Scanning parameters: -1.2V, 0.1 nA

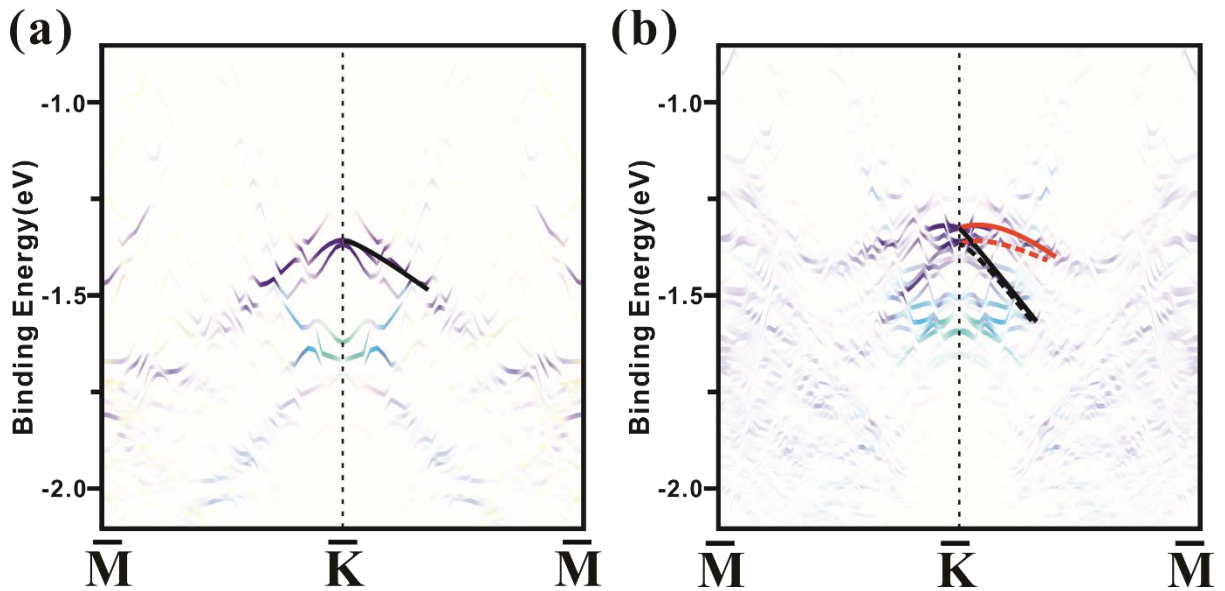


Fig. S2 comparison between calculated band dispersion along  $\bar{K} - \bar{M}$  direction without SOC (a) and with SOC (b) around  $\bar{K}$  point to illustrate the splitting of two pair of Rashba-type band using a  $3 \times \sqrt{3}$  model of the Sb/Au(111) surface reconstruction without buckling of Sb topmost layer. yellow, blue, pink and purple symbols show contributions from  $p_z$ ,  $p_x$ ,  $p_y$  and  $p_x+p_y$  states, respectively.